SCIENTIFIC REPORTS

OPEN

SUBJECT AREAS:
ELECTRONIC DEVICES
ELECTRICAL AND ELECTRONIC ENGINEERING

Received
15 July 2014

Accepted
26 August 2014

Published
22 September 2014

Correspondence and requests for materials should be addressed to J.L. (liu.jiangwei@nims.go.jp)

Low on-resistance diamond field effect transistor with high-*k* ZrO_2 as dielectric

Jiangwei Liu[1], Meiyong Liao[2], Masataka Imura[2], Akihiro Tanaka[3], Hideo Iwai[3] & Yasuo Koide[2,4,5]

[1]International Center for Young Scientists, National Institute for Materials Science (NIMS), 1-1 Namiki, Tsukuba, Ibaraki 305-0044, Japan, [2]Optical and Electronic Materials Unit, NIMS, 1-1 Namiki, Tsukuba, Ibaraki 305-0044, Japan, [3]Materials Analysis Station, NIMS, 1-2-1 Sengen, Tsukuba, Ibaraki 305-0047, Japan, [4]Nanofabrication Platform, NIMS, 1-2-1 Sengen, Tsukuba, Ibaraki 305-0047, Japan, [5]Center of Materials Research for Low Carbon Emission, NIMS, 1-1 Namiki, Tsukuba, Ibaraki 305-0044, Japan.

Although several high-*k* insulators have been deposited on the diamond for metal-insulator-semiconductor field effect transistors (MISFETs) fabrication, the *k* values and current output are still not fully satisfactory. Here, we present a high-*k* ZrO_2 layer on the diamond for the MISFETs. The *k* value for ZrO_2 is determined by capacitance-voltage characteristic to be 15.4. The leakage current density is smaller than 4.8×10^{-5} A·cm^{-2} for the gate voltage ranging from -4.0 to 2.0 V. The low on-resistance MISFET is obtained by eliminating source/drain-channel interspaces, which shows a large current output and a high extrinsic transconductance. The high-performance diamond MISFET fabrication will push forward the development of power devices.

Recently, wide band gap semiconductors such as SiC, GaN, and diamond have been developed in order to replace silicon partly for power devices due to their high carrier mobility and high breakdown field[1–3]. In particular, the diamond is considered to be an ideal material for the application of power devices due to its theoretical low power-loss at a high voltage[4]. However, there is a great issue for the development of the diamond-based electronic devices. Activation energies for the diamond dopants (such as 370 meV for boron) are much larger than thermal energy at room temperature (26 meV)[5]. Although boron δ-doped diamond was considered to be a promising channel layer for metal-insulator-semiconductor field effect transistors (MISFETs)[6–8], its mobility was behind expectations. On the other hand, most of successful diamond-based FETs have been fabricated on hydrogenated-diamond (H-diamond) epitaxial layers, which accumulate two-dimensional hole gases (2DHGs) on the surface with sheet hole density of 10^{12}–10^{13} cm^{-2} [9,10].

Since the insulator with a higher-dielectric constant (higher-*k*) can provide the relatively large charge response at a smaller electrical field[11], it is promising to fabricate the high-*k* insulator on the H-diamond. Several gate insulators such as SiO_2, AlN, Al_2O_3, and CaF_2 have been deposited on the H-diamond for fabricating the MISFETs[12–15]. However, the *k* values of them are not large. Although sputtering-deposited Ta_2O_5[11] and atomic-layer-deposited HfO_2[16] had higher-*k* than other materials mentioned above, the high density of trapped and fixed charges in both the oxides made them difficult for the applications of the MISFETs. Our group demonstrated the normally-off HfO_2-gated MISFET with $k = 9.4$ using the bilayer HfO_2 structure prepared by atomic layer deposition (ALD) and sputtering deposition (SD) techniques[17]. This bilayer gate strategy was also applied to $LaAlO_3/Al_2O_3$-gated MISFET with $k = 9.1$[18]. Although these MISFETs showed good electrical properties, the *k* value was still not large. Recently, we have deposited SD-Ta_2O_5/ALD-Al_2O_3 on the H-diamond for MIS diode and MISFET[19]. The *k* value of the SD-Ta_2O_5/ALD-Al_2O_3 is around 12.7, which is larger than those of the SD-HfO_2/ALD-HfO_2 and SD-$LaAlO_3$/ALD-Al_2O_3. However, the leakage current density (*J*) and fixed charge density were high. Thus, a new high-*k* insulator should be developed for the high-performance H-diamond-based MISFETs.

Since ZrO_2 has a high-*k* (25), a wide band gap (5.8 eV), and a large breakdown field (15–20 MV·cm^{-1})[20], it is possibly a good candidate for the H-diamond-based MISFETs. Several deposition techniques such as atomic layer deposition (ALD)[21], molecular beam evaporation[22], chemical vapor deposition[23], pulsed laser deposition[24], and sputtering deposition (SD)[25,26] have been used for the ZrO_2 fabrication. The ZrO_2 layer deposited on Si substrate by the SD technique was reported to show small leakage current and low trapped charge densities[26]. Thus, it is promising to deposit high-quality ZrO_2 layer on the H-diamond by the SD technique. However, since the H-diamond surface is predicted to be damaged easily by plasma discharge during the SD deposition, a buffer layer is necessary to keep the 2DHG in the H-diamond. The Al_2O_3 deposited by the ALD technique was reported to be a large valence band offset[27] against the H-diamond and was confirmed to be the effective buffer layer for the SD-

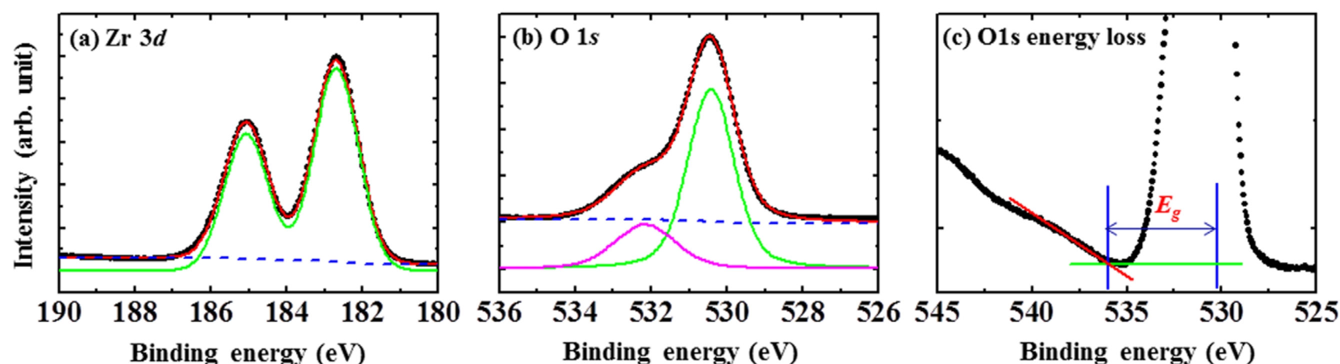

Figure 1 | **XPS spectra of ZrO_2 layer.** (a) Zr 3*d*, (b) O 1 *s*, and (c) O 1 *s* photoelectron energy loss spectra for the SD-ZrO_2 (32.5 nm) layer. The Zr 3*d* and O 1 *s* core level spectra were fitted by Voigt (mixed Lorenzian-Gaussian) lineshapes after the application of Shirley background (dashed line). The solid lines matched to the dots are the sums of Voigt lineshapes and background.

$LaAlO_3$ on the H-diamond[18]. Therefore, the SD-ZrO_2/ALD-Al_2O_3 bilayer oxide insulator would be promising for the application of the H-diamond-based MISFET.

On the other hand, since on-resistance (R_{ON}) of the MISFET can affect the current density and power-loss, our effort is to reduce the R_{ON} for the H-diamond-based MISFET. The R_{ON} value is usually composed of source/drain electrode contact resistance (R_C), channel resistance beneath the oxide films (R_{CH}), and source/drain-channel resistance (R_{SD})[14,17,18]. The R_C is controlled by the metal contact to the 2DHG in the H-diamond, which is much smaller than the R_{CH} and R_{SD}. The R_{CH} is directly related to the intrinsic properties (hole density and mobility) of the H-diamond. Some studies have focused on the increasing of hole density by the H-diamond surface treatment, which decreases the R_{CH} and improve the electrical properties of the MISFETs[13,14]. However, there are few studies on the topic of R_{SD} decreasing. Almost all the H-diamond-based MISFETs have source/drain-channel interspaces ($I_{S/D-CH}$)[14,17,18], which implies the existence of large R_{SD}. Therefore, the H-diamond-based MISFET without the $I_{S/D-CH}$ is strongly required to be fabricated. Recently, we have fabricated SD-Ta_2O_5/ALD-Al_2O_3-gated H-diamond MISFET to reduce the R_{ON} by eliminating $I_{S/D-CH}$[19]. However, the current output was still not satisfactory.

In this reports, chemical and electrical properties of the high-*k* ZrO_2 on the H-diamond are investigated. In addition, the SD-ZrO_2/ALD-Al_2O_3-gated H-diamond MISFET with a low R_{ON} and large output current is demonstrated. The *k* values for the SD-ZrO_2/ALD-Al_2O_3 bilayer and single SD-ZrO_2 layer are determined by capacitance-voltage (C-V) characteristic to be 12.8 and 15.4, respectively. The drain-source current maximum (I_{DSmax}) for the MISFET without $I_{S/D-CH}$ is as large as -224.1 mA·mm^{-1}.

Results

Chemical properties of ZrO_2 layer. Figure 1 shows spectra of the Zr 3*d*, O 1 *s*, and O 1 *s* photoelectron energy loss peak for the amorphous SD-ZrO_2 (32.5 nm) layer measured by x-ray photoelectron spectroscopy (XPS). The Zr 3*d* and O 1 *s* core level spectra were fitted by Voigt (mixed Lorenzian-Gaussian) lineshapes with Shirley background (dashed line). The solid lines matched to the dots were the sums of Voigt lineshapes and background. All the photoelectron spectra were calibrated relative to the reference C 1 *s* peak position (285.0 eV). The Zr 3*d* spectrum [Fig. 1 (a)] had the strong spin-orbit doublet Zr $3d_{5/2}$-Zr $3d_{3/2}$ with splitting of 2.3 eV. It was fitted by a single component (Zr-O) with the binding energy of 182.7 ± 0.2 eV for the Zr $3d_{5/2}$. To fit O 1 *s* spectrum [Fig. 1 (b)], two components (O-Zr and O-H) were required. The binding energies for them were 530.4 ± 0.2 and 532.2 ± 0.2 eV, respectively. Based on the intensity ratio of the Zr $3d_{5/2}$ to O 1 *s* and the inelastic mean free paths for them[28], the atomic ratio between zirconium and oxygen can be calculated to be 1 : 2. Thus, we obtained the stoichiometric SD-ZrO_2 layer on the H-diamond surface. The band gap energy (E_g) of the ZrO_2 was determined by the O 1 *s* photoelectron energy loss peak [Fig. 1 (c)]. Threshold energy[29,30] of the O 1 *s* photoelectron energy loss peak was determined by extrapolating a linear fit of the leading edge to the baseline to be 536.0 ± 0.2 eV. According to the O 1 *s* core level binding energy (530.4 ± 0.2 eV) for the O-Zr bonds, the E_g of amorphous ZrO_2 layer was determined to be 5.6 ± 0.4 eV, which was in good agreement with the other literature datum (5.8 eV)[31].

Electrical properties of MIS diode. Figure 2 (a) shows the *J* for the SD-ZrO_2/ALD-Al_2O_3/H-diamond MIS diode for gate voltage ranging from -4.0 to 2.0 V. The inset in the Fig. 2 (a) is the top view of the planar-type MIS diode. The *J* was obtained with dividing leakage current by area of the gate electrode (1.77×10^{-4} cm^2). With the change of the gate bias from positive to negative, the *J* value increases to 4.8×10^{-5} A·cm^{-2} at -4.0 V. The obvious accumulation and depletion regions are observed in the C-V curve [Fig. 2 (b)]. The maximum capacitance is 0.310 μF·cm^{-2}. Based on

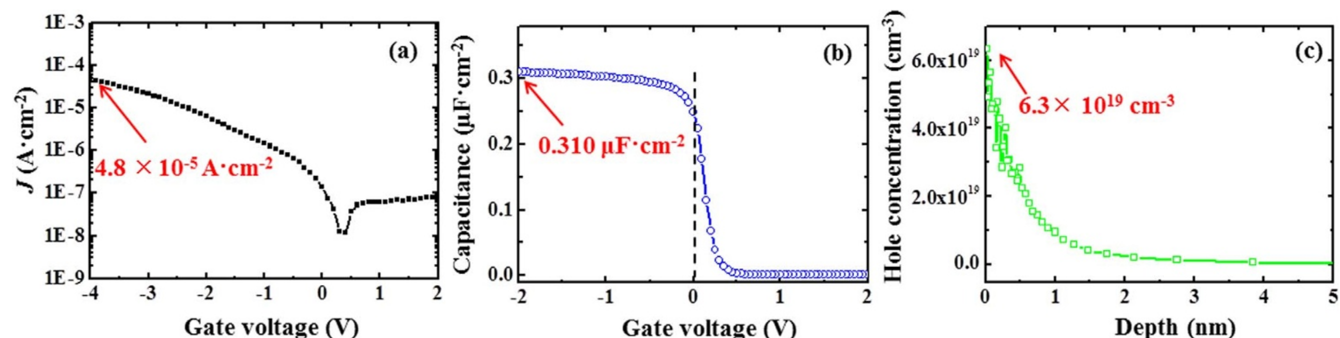

Figure 2 | **Electrical properties of the MIS diode.** (a) The *J*-V and (b) the C-V curves for the SD-ZrO_2/ALD-Al_2O_3/H-diamond MIS diode. (c) Hole concentration of the H-diamond channel layer as a function of depth from the ALD-Al_2O_3/H-diamond interface to the H-diamond epitaxial layer.

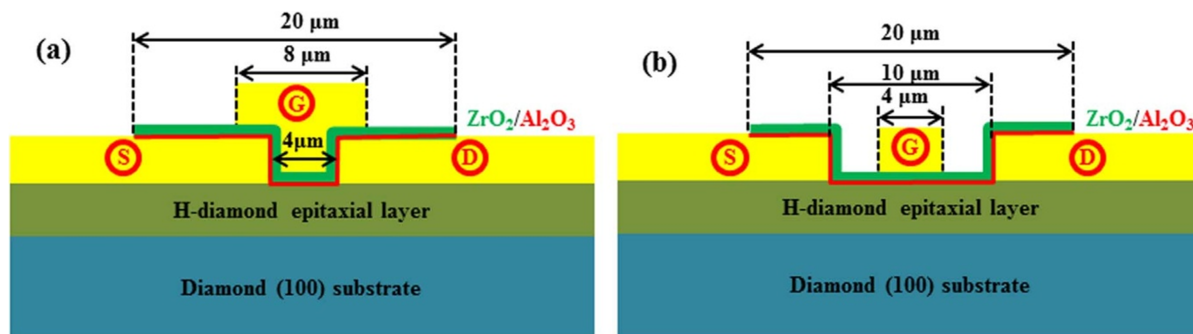

Figure 3 | Schematic cross-sectional structures of the SD-ZrO_2/ALD-Al_2O_3/H-diamond MISFETs. (a) Without and (b) with $I_{S/D-CH}$.

this value and the total oxide bilayer thickness (36.5 nm), the *k* value of the SD-ZrO_2/ALD-Al_2O_3 bilayer can be calculated to be 12.8, which is larger than those of the SD-$LaAlO_3$/ALD-Al_2O_3 (9.1), SD-HfO_2/ALD-HfO_2 (9.4), ALD-HfO_2 (12.1), and SD-Ta_2O_5/ALD-Al_2O_3[16–18]. According to the *k* value of 5.4 and the thickness of 4.0 nm for the ALD-Al_2O_3 on the H-diamond (Data shown in the supporting information), the *k* value for the single SD-ZrO_2 can be calculated to be as large as 15.4. The C-V curve shows small flat band voltage (V_{FB}) shift and small stretch-out[32] in the depletion region, which implies low fixed and trapped charge densities in the SD-ZrO_2/ALD-Al_2O_3/H-diamond structure[33,34]. Based on the C-V curve and profiling technique[13,35], the 2DHG density as a function of depth from the ALD-Al_2O_3/H-diamond interface to the H-diamond epitaxial layer can be determined, which is shown in Fig. 2 (c). The peak hole density is 6.3×10^{19} cm^{-3}. With increasing the depth, the hole density decreases quickly, which indicates the existence of 2DHG in the H-diamond epitaxial layer close to the ALD-Al_2O_3/H-diamond interface. Assuming the 2DHG region with 1 nm thickness, the sheet hole density (p_{CV}) is evaluated to be 3.15×10^{12} cm^{-2}.

Electrical properties of MISFETs. Figure 3 shows schematic cross-sectional structures of the SD-ZrO_2/ALD-Al_2O_3/H-diamond MISFETs without [Fig. 3 (a)] and with [Fig. 3 (b)] $I_{S/D-CH}$. The MISFET without $I_{S/D-CH}$ in Fig. 3 (a) has the T-shaped gate electrode with top and bottom lengths of 8 and 4 µm, respectively. The MISFET with $I_{S/D-CH}$ in Fig. 3 (b) has an interspace of 3 µm between gate and source/drain contacts. The gate length (L_G) and gate width (W_G) are 4 and 150 µm, respectively. Figs. 4 (a)$_0$ and (b)$_0$ show drain/source current versus voltage (I_{DS}-V_{DS}) characteristics for the SD-ZrO_2/ALD-Al_2O_3/H-diamond MISFETs without and with $I_{S/D-CH}$, respectively. The gate voltage (V_{GS}) was varied from -4.0 to 2.0 V in steps of +0.5 V. Both the MISFETs show *p*-type channel characteristics. The I_{DSmax} for the MISFET without $I_{S/D-CH}$ is -224.1 mA·mm^{-1}, which is much larger than that for the MISFET with $I_{S/D-CH}$ of -29.3 mA·mm^{-1}. The R_{ON} can be extracted from the linear region of the I_{DS}-V_{DS} characteristics. It is 29.7 Ω·mm for the MISFET without $I_{S/D-CH}$. This value is much smaller than that of 208.4 Ω·mm for the MISFET with $I_{S/D-CH}$. The transfer characteristics corresponding to the I_{DS}-V_{DS} curves are shown in the Figs. 4 (a, b)$_{1,2}$. Threshold voltage (V_{TH}) for the MISFET with $I_{S/D-CH}$ was 1.3 ± 0.1 V, which almost equals to the value of 1.4 ± 0.1 V for the MISFET without $I_{S/D-CH}$. The extrinsic transconductance (g_m) was determined based on the slope of the linear portion for the I_{DS}-V_{GS} curves. The values of the g_m maximum ($g_{m,max}$) for the MISFETs without and with $I_{S/D-CH}$ are 70.4 ± 0.1 and 10.1 ± 0.1 mS·mm^{-1}, respectively.

The effective mobility (μ_{eff}) for the H-diamond channel layer can be calculated by the following equation with conditions of $R_C \ll R_{SD}$, R_{CH},

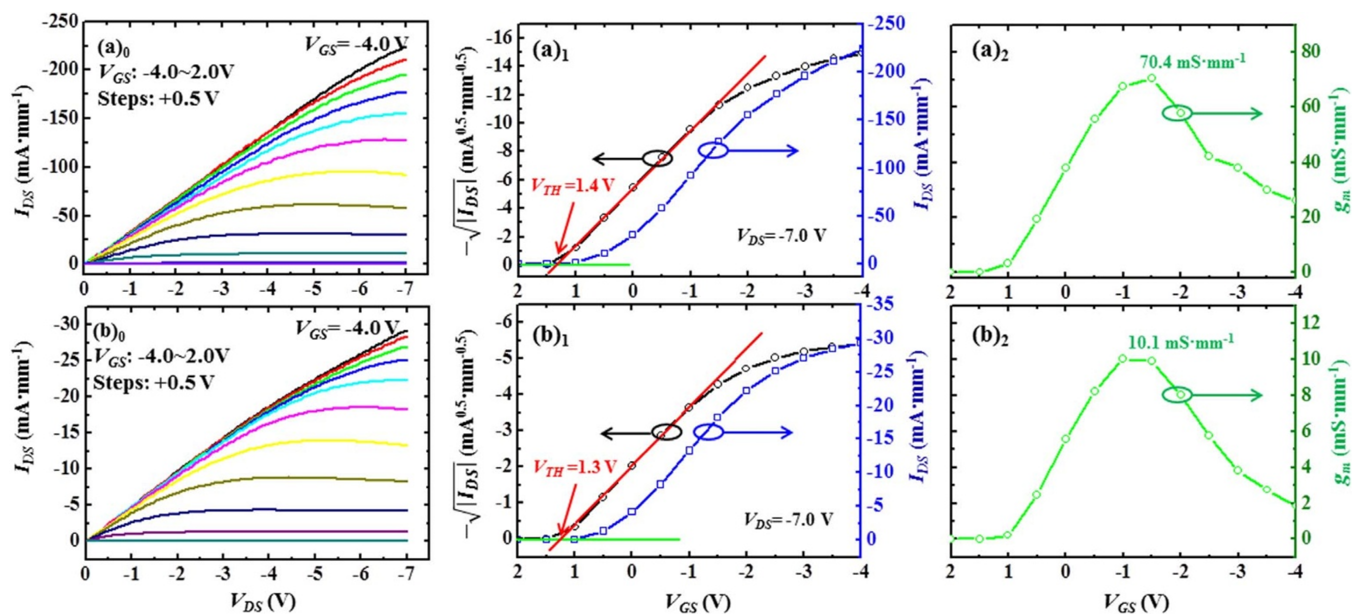

Figure 4 | Electrical properties of the MISFETs. The I_{DS}-V_{DS}, I_{DS}-V_{GS}, $-\sqrt{|I_{DS}|}$-V_{GS}, and g_m-V_{GS} characteristics of the SD-ZrO_2/ALD-Al_2O_3/H-diamond MISFETs without [Figs. 4 (a)$_{0,1,2}$] and with [Figs. 4 (b)$_{0,1,2}$] $I_{S/D-CH}$.

Table 1 | Electrical properties of the SD-ZrO_2/ALD-Al_2O_3/H-diamond MISFETs

MISFET	R_{ON} [Ω·mm]	I_{DSmax} [mA·mm^{-1}]	V_{TH} [V]	$g_{m,max}$ [mS·mm^{-1}]
Without $I_{S/D\text{-}CH}$	29.7	−224.1	1.3 ± 0.1	70.4
With $I_{S/D\text{-}CH}$	208.4	−29.3	1.4 ± 0.1	10.1

$$I_{DS} = \frac{W_G \mu_{eff} C_{OX}}{L_G} \left\{ (V_{GS} - V_{TH}) V_{DS} - \frac{1}{2} V_{DS}^2 \right\}, \quad (1)$$

where the W_G, L_G, C_{OX}, I_{DS}, and V_{TH} have been mentioned above to be 150 μm, 4 μm, 0.310 μF·cm^{-2}, −224.1 mA·mm^{-1}, and 1.4 ± 0.1 V, respectively. The μ_{eff} was calculated to be 217.5 ± 0.5 cm^2·V^{-1}·s^{-1} at the V_{DS} of −7.0 V. Based on the μ_{eff} value, the sheet hole density (p_{IV}) for the H-diamond channel can be calculated by the following equation,

$$\mu_{eff} = \frac{1}{q p_{IV} R_{CHsheet}}, \quad (2)$$

where the q is the charge of one electron (1.6 ×10^{-19} C). The $R_{CHsheet}$ is the sheet resistance of the H-diamond channel layer, which was determined to be 7.46 × 10^3 Ω/□. Thus, the p_{IV} can be calculated to be 3.74 ×10^{12} cm^{-2}, which is close to the p_{CV} and reasonable for the common H-diamond.

Discussion

The electrical properties of the SD-ZrO_2/ALD-Al_2O_3/H-diamond MISFETs without and with $I_{S/D\text{-}CH}$ were summarized in the table 1. The R_{ON} for the MISFET without $I_{S/D\text{-}CH}$ is almost seven times smaller than the one with $I_{S/D\text{-}CH}$. Therefore, the I_{DSmax} and $g_{m,max}$ values for the MISFET without $I_{S/D\text{-}CH}$ are almost seven times larger than those with $I_{S/D\text{-}CH}$. The reduction of R_{SD} has obviously decreased the R_{ON} and significantly improved the electrical properties of the H-diamond-based MISFETs. Recently, the highest I_{DSmax} was reported by Hirama *et al.* to be −600 mA·mm^{-1} at L_G = 4 μm for the ALD-Al_2O_3-gated H-diamond MISFET[14], which is larger than our present value of −224.1 mA·mm^{-1}. This is attributed to the higher sheet hole density of 4 × 10^{13} cm^{-2} for the H-diamond epitaxial layer treated by NO_2 ambient than the as-grown one of 3.74 ×10^{12} cm^{-2} in this report. It is believed that the increment of the hole density will possibly provide the highest I_{DSmax} in the future.

Table 2 summarized our recent reports for the electrical properties of the insulator/diamond MISFETs. The SD-Ta_2O_5 and ALD-HfO_2 on the diamond showed k values larger than 12.1[11,16]. However, they were difficult to operate the MISFETs because the high trapped and fixed charge densities were existed in both the oxides. Although the SD-$LaAlO_3$/ALD-Al_2O_3/H-diamond and SD-HfO_2/ALD-HfO_2/H-diamond MISFETs showed good electrical properties[13,17,18], the k values of them were smaller than 9.4. Recently, the SD-Ta_2O_5/ALD-Al_2O_3 bilayer has been deposited on the H-diamond for the MISFETs. The k values of SD-Ta_2O_5/ALD-Al_2O_3 and single SD-Ta_2O_5 were as large as 12.7 and 16.5, respectively[19]. The I_{DSmax} was −97.7 mA·mm^{-1}, which was larger than those of the SD-$LaAlO_3$/ALD-Al_2O_3/H-diamond and SD-HfO_2/ALD-HfO_2/H-diamond MISFETs due to the eliminating of $I_{S/D\text{-}CH}$. However, the J of SD-Ta_2O_5/ALD-Al_2O_3/H-diamond MIS diode was one order larger than that of the SD-ZrO_2/ALD-Al_2O_3 MIS diode. In addition, the fixed charge density in the SD-Ta_2O_5/ALD-Al_2O_3 was higher than that in the SD-ZrO_2/ALD-Al_2O_3.

In conclusion, the chemical and electrical properties of the high-k SD-ZrO_2/ALD-Al_2O_3 layer on the H-diamond were investigated. The atomic ratio between zirconium and oxygen of the SD-ZrO_2 layer and E_g were determined by XPS to be 1 : 2 and 5.6 ± 0.4 eV, respectively. The J of the MIS diode was smaller than 4.8 × 10^{-5} A·cm^{-2}. The k values of the SD-ZrO_2/ALD-Al_2O_3 bilayer and single SD-ZrO_2 layer were determined to be as large as 12.8 and 15.4, respectively. The R_{ON}, I_{DSmax}, $g_{m,max}$, μ_{eff}, and p_{IV} for the MISFET without $I_{S/D\text{-}CH}$ were 29.7 Ω·mm, −224.1 mA·mm^{-1}, 70.4 ± 0.1 mS·mm^{-1}, 217.5 ± 0.5 cm^2·V^{-1}·s^{-1}, and 3.74 × 10^{12} cm^{-2}, respectively.

Methods

H-diamond, Al_2O_3, and ZrO_2 depositions. The H-diamond homoepitaxial layer was deposited by a microwave plasma-enhanced chemical vapor deposition on the Ib-type single crystalline diamond (100) substrate with dimension of 2.5 × 2.5 × 0.5 mm^3. In order to remove remaining contaminations on the surface of the diamond, the substrate was firstly annealed at 1000°C for 20 min in an ambient of H_2. The deposition temperature and chamber pressure for the H-diamond were 900 ~ 940°C and 80 Torr, respectively. The H_2 and CH_4 flow rates were 500 and 0.5 sccm, respectively. Thickness of the H-diamond epitaxial layer was about 200 nm. The ALD-Al_2O_3 buffer layer with thickness of 4.0 nm was deposited using precursors of $Al(CH_3)_4$ and water vapor at 120°C. The pulse and purge times for them were 0.1 and 4.0 s, respectively. The SD-ZrO_2 film with thickness of 32.5 nm was deposited on the ALD-Al_2O_3/H-diamond by the radio-frequency (RF) SD technique in a pure argon-atmosphere at room temperature. The RF power was 30 W and the chamber pressure was kept at 1 Pa. Thicknesses of the ALD-Al_2O_3 and SD-ZrO_2 was determined by ellipsonmeter. The XPS measurements for the SD-ZrO_2 were performed by a monochromated Al Kα X-ray source ($h\nu$ = 1486.6 eV) with a vacuum pressure of 1.0 × 10^{-9} Torr. Each spectrum was recorded with a 0.05 eV step and a 55 eV pass energy.

MIS diode fabrication. The gate and ohmic contact electrodes were deposited on the surfaces of the SD-ZrO_2/ALD-Al_2O_3 and H-diamond using an electron-beam evaporator, respectively. The diameter of the circular SD-ZrO_2/ALD-Al_2O_3 film and gate electrode was 150 μm with an interspacing of 10 μm between the SD-ZrO_2/ALD-Al_2O_3 and the ohmic Au/Ti/Pd contact (Schematic cross-sectional structure of the MIS diode shown in the supporting information). The current-voltage and C-V measurements for the MIS diode were performed at room temperature under dark condition. The frequency for the C-V measurement was 50 kHz with voltage steps of 0.1 V.

MISFETs fabrication. The fabrication of the SD-ZrO_2/ALD-Al_2O_3/H-diamond MISFETs was based on the combinations of laser lithography, dry-etching, an ALD technique, a SD technique, electrodes metallization, and lift-off technique. There are mainly three steps (Fabrication process shown in the supporting information): I. mesa-structure fabrication, II. source/drain ohmic contact fabrication, and III. gate oxide and contact fabrication. The photoresists of LOR5A and AZ5214E were used

Table 2 | Summary of our recent reports for the electrical properties of the insulator/diamond MISFETs[11,16-19].

Oxide insulator	k	W_G (μm)	L_G (μm)	$I_{S/D\text{-}CH}$ (μm)	R_{ON} (Ω·mm)	I_{DSmax} (mA·mm^{-1})
ALD-HfO_2	12.1	-	-	-	-	-
SD-Ta_2O_5	16.0	-	-	-	-	-
SD-$LaAlO_3$/ALD-Al_2O_3	9.1	150	10	15	637	−7.5
SD-HfO_2/ALD-HfO_2	9.4	150	4	10	230	−38.7
SD-Ta_2O_5/ALD-Al_2O_3	12.7	150	4	0	42.9	−97.7
SD-ZrO_2/ALD-Al_2O_3	12.8	150	4	5	208.4	−29.3
				0	29.7	−224.1

for all the patterning processes. After coating the photoresist, the sample was exposed by 405 nm illumination using the laser lithography system and then was developed in a tetramethylammonium hydroxide solution. The H-diamond channel layer was etched under O_2 atmosphere with pressure of 10 Pa by reactive ion etching system in order to fabricate the mesa-structure. The ALD-Al_2O_3 buffer layer and SD-ZrO_2 layer were subsequently deposited on the H-diamond surface. Note that the oxide insulators were patterned by the photoresists, which made the MISFET without $I_{S/D\text{-}CH}$ fabricated successfully. After the finishing each fabrication step, the photoresists were removed by an N-methylpyrrolidone solution at room temperature. The electrical properties of the SD-ZrO_2/ALD-Al_2O_3/H-diamond MISFETs were measured under a dark condition using high performance MX-200/B prober and B1500A parameter analyzer.

1. Hino, S. *et al*. High channel mobility 4H-SiC metal-oxide-semiconductor field-effect transistor with low temperature metal-organic chemical-vapor deposition grown Al_2O_3 gate insulator. *Appl. Phys. Lett.* **92**, 183503 (2008).
2. Ye, P. D. *et al*. GaN metal-oxide-semiconductor high-electron-mobility-transistor with atomic layer deposited Al_2O_3 as gate dielectric. *Appl. Phys. Lett.* **86**, 063501 (2005).
3. Dankerl, M. *et al*. Diamond transistor array for extracellular recording from electrogenic cells. *Adv. Funct. Mater.* **19**, 2915–2923 (2009).
4. Baliga, J. Power Semiconductor Device Figure of Merit for High Frequency Applications. *IEEE Electron Device Letters* **10**, 455–457 (1989).
5. Walker, J. Optical absorption and luminescence in diamond. *Rep. Prog. Phys.* **42**, 1605–1659 (1979).
6. Kueck, D., Hajj, H. E., Kaiser, A. & Kohn, E. Surface-channel MESFET with boron-doped contact layer. *Diamond Relat. Mater.* **17**, 732–735 (2008).
7. Haji, H. E., Denisenko, A., Kaiser, A., Balmer, R. S. & Kohn E. Characteristics of boron δ-doped diamond for electronic applications. *Diamond Relat. Mater.* **17**, 409–414 (2008).
8. Edgington, R. *et al*. H. Growth and electrical characterization of δ-doped boron layers on (111) diamond surfaces. *J. Appl. Phys.* **111**, 033710 (2012).
9. Kawarada, H., Araki, Y., Sakai, T., Ogawa, T. & Umezawa, H. Electrolyte-solution-gate FETs using diamond surface for biocompatible ion sensors. *Phys. Status Solidi (a)* **185**, 79–83 (2001).
10. Rezek, B., Watanabe, H. & Nebel, C. E. High carrier mobility on hydrogen terminated 100 diamond surfaces. *Appl. Phys. Lett.* **88**, 042110 (2006).
11. Cheng, S. H. *et al*. Integration of high-dielectric constant Ta_2O_5 oxides on diamond for power devices. *Appl. Phys. Lett.* **101**, 232907 (2012).
12. Saito, T. *et al*. Fabrication of metal-oxide-diamond field-effect-transistors with submicron-sized gate length on boron-doped (111) H-terminated surfaces using electron beam evaporated SiO_2 and Al_2O_3. *J. Electron. Mater.* **40**, 247–252 (2011).
13. Imura, M. *et al*. Demonstration of diamond field effect transistors by AlN/diamond heterostructure. *Phys. Status Solidi RRL* **5**, 125–127 (2011).
14. Hirama, K., Sato, H., Harada, Y., Yamamoto, H. & Kasu M. Diamond field-effect transistors with 1.3 A/mm drain current density by Al_2O_3 passivation layer. *Jpn. J. Appl. Phys.* **51**, 090112 (2012).
15. Otsuka, Y., Suzuki, S., Shikama, S., Maki, T. & Kobayashi T. Fermi level pinning in metal-insulator-diamond structures. *Jpn. J. Appl. Phys.* **34**, L551–L554 (1995).
16. Liu, J. W. *et al*. Electrical characteristics of hydrogen-terminated diamond metal-oxide-semiconductor with atomic layer deposited HfO_2 as gate dielectric. *Appl. Phys. Lett.* **102**, 112910 (2013).
17. Liu, J. W., Liao, M. Y., Imura, M. & Koide Y. Normally-off HfO_2-gated diamond field effect transistors. *Appl. Phys. Lett.* **103**, 092905 (2013).
18. Liu, J. W. *et al*. Interfacial band configuration and electrical properties of $LaAlO_3$/Al_2O_3/hydrogenated-diamond metal-oxide-semiconductor field effect transistors. *J. Appl. Phys.* **114**, 084108 (2013).
19. Liu, J. W. *et al*. Diamond field effect transistors with a high-dielectric constant Ta_2O_5 as gate material. *J. Phys. D: Appl. Phys.* **47**, 245102 (2014).
20. Chatterjee, S., Nandi, S. K., Maikap, S., Samanta, S. K. & Maiti, C. K. Electrical properties of deposited ZrO_2 films on ZnO/n-Si substrates. *Semicond. Sci. Technol.* **18**, 92–96 (2003).
21. Lee, J., Koo, J., Sim, H. S. & Jeon H. Characteristics of ZrO_2 films deposited by using the atomic layer deposition method. *J. Korean Phys. Soc.* **44**, 915–919 (2004).
22. Maria, J. P. *et al*. High temperature stability in lanthanum and zirconia-based gate dielectrics. *J. Appl. Phys.* **90**, 3476–3482 (2001).
23. Liao, L. *et al*. High-performance top-gated graphene-nanoribbon transistors using zirconium oxide nanowires as high-dielectric-constant gate dielectrics. *Adv. Mater.* **22**, 1941–1945 (2010).
24. Yamaguchi, T., Satake, H., Fukushima, N. & Toriumi, A. Study on Zr-silicate interfacial layer of ZrO_2 metal-insulator-semiconductor structure. *Appl. Phys. Lett.* **80**, 1987–1989 (2002).
25. Gueorguiev, V. K., Aleksandrova, P. V., Ivanov, T. E. & Koprinaro, J. B. Hysteresis in metal insulator semiconductor structures with high temperature annealed ZrO_2/SiO_x layers. *Thin Solid Films* **517**, 1815–1820 (2009).
26. Prabakar, K. *et al*. rf-Magnetron sputter deposited ZrO_2 dielectrics for metal-insulator-semiconductor capacitors. *Vacuum* **82**, 1367–1370 (2008).
27. Liu, J. W., Liao, M. Y., Imura, M. & Koide, Y. Band offsets of Al_2O_3 and HfO_2 oxides deposited by atomic layer deposition technique on hydrogenated diamond. *Appl. Phys. Lett.* **101**, 252108 (2012).
28. Zhang, L., Wett, D., Szargan, R. & Chassé, T. Determination of ZnO(0001) surface termination by x-ray photoelectron spectroscopy at photoemission angles of 0° and 70°. *Surf. Interface Anal.* **36**, 1479–1483 (2004).
29. Miyazaki, S. Photoemission study of energy-band alignments and gap-state density distributions for high-*k* gate dielectrics. *J. Vac. Sci. Technol. B* **19**, 2212–2215 (2001).
30. Reiche, R., Yubero, F., Espinós, J. P. & González-Elipe, A. R. Structure, microstructure and electronic characterization of the Al_2O_3/SiO_2 interface by electron spectroscopies. *Surf. Sci.* **457**, 199–210 (2000).
31. Sayan, S. *et al*. Valence and conduction band offsets of a ZrO_2/SiO_xN_y/n-Si CMOS gate stack: A combined photoemission and inverse photoemission study. *Phys. Status Solidi (b)* **241**, 2246–2252 (2004).
32. Bae, C., Krug, C. & Lucovsky G. Electron trapping in metal-insulator-semiconductor structures on n-GaN with SiO_2 and Si_3N_4 dielectrics. *J. Vac. Sci. Technol. A* **22**, 2379–2383 (2004).
33. Hu, W. D. *et al*. Self-heating simulation of GaN-based metal-oxide-semiconductor high-electron-mobility transistors including hot electron and quantum effects. *J. Appl. Phys.* **100**, 074501 (2006).
34. Hu, W. D. *et al*. Simulation and optimization of GaN-based metal-oxide-semiconductor high-electron-mobility-transistor using field-dependent drift velocity model. *J. Appl. Phys.* **102**, 034505 (2007).
35. Ambacher, O. *et al*. Two-dimensional electron gases induced by spontaneous and piezoelectric polarization charges in N-and Ga-face AlGaN/GaN heterostructures. *J. Appl. Phys.* **85**, 3222–3233 (1999).

Acknowledgments

This work was supported by the International Center for Young Scientists (ICYS) of the National Institute for Materials Science (NIMS). It was also supported in part by Tokodai Institute for Elemental Strategy (TIES), Advanced Environmental Materials, Green Network of Excellence (GRENE), Low-Carbon Research Network (LCnet), and Nanotechnology Platform projects sponsored by the Ministry of Education, Culture, Sports, and Technology (MEXT) in Japan.

Author contributions

J.L. designed and carried out the experiments. A.T. and H.I. performed XPS measurement. J.L., Y.K., M.L., and M.I. substantially contributed to interpreting the results and writing the paper.

Additional information

Supplementary information accompanies this paper at http://www.nature.com/scientificreports

Competing financial interests: The authors declare no competing financial interests.

How to cite this article: Liu, J. *et al*. Low on-resistance diamond field effect transistor with high-*k* ZrO_2 as dielectric. *Sci. Rep.* **4**, 6395; DOI:10.1038/srep06395 (2014).

This work is licensed under a Creative Commons Attribution-NonCommercial-NoDerivs 4.0 International License. The images or other third party material in this article are included in the article's Creative Commons license, unless indicated otherwise in the credit line; if the material is not included under the Creative Commons license, users will need to obtain permission from the license holder in order to reproduce the material. To view a copy of this license, visit http://creativecommons.org/licenses/by-nc-nd/4.0/